Date of publication xxxx 00, 0000, date of current version October xx, 2017.

Digital Object Identifier 10.1109/ACCESS.2017.DOI

3-D Spatial Modeling of Network Interference in Two-Tier Heterogeneous Networks

SYED JUNAID NAWAZ[1], (Senior Member, IEEE), ABRAR AHMED[1], SHURJEEL WYNE[1], (Senior Member, IEEE), KANAPATHIPPILLAI CUMANAN[2], (Member, IEEE), and ZHIGUO DING[3], (Senior Member, IEEE).

[1]Department of Electrical Engineering, COMSATS Institute of Information Technology, Islamabad, Pakistan, (e-mail: junaidnawaz@ieee.org, abrar_ahmed@comsats.edu.pk, shurjeel.wyne@comsats.edu.pk)
[2]Department of Electronic Engineering, University of York, UK (e-mail: kanapathippillai.cumanan@york.ac.uk).
[3]School of Computing and Communications, Lancaster University, UK (e-mail: z.ding@lancaster.ac.uk).

Syed Junaid Nawaz (e-mail: junaidnawaz@ieee.org).

This work was supported by EU ATOM-690750 research project approved under the call identifier H2020-MSCA-RISE-2015.

ABSTRACT The multi-tier heterogeneous network (HetNet) architecture can potentially address the massive connectivity and high throughput demands of the emerging fifth generation (5G) of wireless networks. However, the inter-tier interference in HetNets is considered to be a major performance bottleneck. This work proposes a geometry-based three-dimensional (3-D) stochastic channel model for the spatial characterization of the sum interference in a two-tier HetNet with small cells in tier-1 overlaid with massive multiple-input-multiple-output (MIMO) equipped macro-cell base stations in tier-2. The angular spreads of the interference and the desired signals are analyzed by using the theory of 3-D multipath shape-factors and analytical expressions are derived for their second-order fading statistics, viz: level-crossing-rate (LCR), average-fade-duration (AFD), spatial autocovariance (SAC), and the coherence distance (CD). Further, analytical expressions to investigate the second-order fading statistics against signal-to-interference ratio (SIR) are also derived. The validation of derived analytical expressions is established through a comparison with performed computer based simulations. To provide insights into the network sum interference mechanism, the LCR and AFD expressions are derived for the special case when the rate of fluctuation of the desired signal is much higher than that of the interference signal and vice versa. Furthermore, the impact of the model's physical parameters such as the link distance and the receiver's direction of motion as well as the fading distribution parameters such as its intensity and shape factors on the fading statistics of the interference are evaluated. These results demonstrate that the elevation angle has a significant impact on the interference characterization in HetNet architectures such that it cannot be ignored in modeling emerging 5G communication scenarios.

INDEX TERMS Interference, Signal-to-interference ratio, Angular Spread, Average-fade-duration, Level-crossing-rate, Spatial correlation, HetNets, massive-MIMO.

I. INTRODUCTION

CELLULAR networks are evolving from planned macro-cell clusters to dense irregularly deployed multi-tier heterogeneous networks (HetNets) in which the macro-cells co-exist with small cells (SCs) such as pico- and/or femto-cells. Despite the network capacity enhancement offered by small cells, the macro-cells cannot be completely replaced due to their offered advantages of serving a large geographic region and providing reliable links to high mobility users [1]. Another technology enabler for the envisioned fifth generation (5G) wireless networks is the concept of massive multiple-input multiple-out (MIMO), which equips the base station (BS) with a very large number of antennas to offer high capacity, improved link reliability, and reduced network interference [2, 3]. Multi-tier HetNets that include SCs in the first-tier overlaid with massive-MIMO equipped macro-cell BSs (MBSs) in the second-tier are believed to be a desirable HetNet architecture for simultaneously reaping the benefits of both these technologies [4]. The main performance bottleneck in such massive-MIMO aided multi-tier HetNets is

the cumulative network interference caused by the reduced separation among the BSs, which leads to aggressive spatial reuse of the radio spectrum [5]. Therefore, accurate modeling and characterization of network interference is of immense importance to fully exploit the benefits of such massive-MIMO aided multi-tier HetNet architectures.

In [6], the authors provided a comprehensive throughput analysis of massive-MIMO aided multi-tier HetNets and suggested that the throughput can be significantly increased by strong coordination between the tiers to exploit interference nulling. The work in [1] proposed a HetNet architecture with SCs overlaid with massive-MIMO enabled MBSs. The authors proposed a method for dedicating a few antennas at the MBSs for suppression of the cumulative interference on the SCs. In [7], a stochastic geometry based model for multi-tier HetNets was analyzed. In [8], a massive-MIMO based multi-tier HetNet architecture was studied and it was suggested that massive-MIMO equipped MBSs can significantly enhance the overall rate and coverage of the network. In [9] a two-tier network architecture with pico-cell overlaid with massive-MIMO equipped MBSs was proposed and the impact of various physical parameters such as the radius of the macro-cell and SC coverage areas on the network's spectral efficiency was thoroughly investigated. In [10], a spatial interference coordination method was proposed for the mitigation of the interference caused from the macro-cells towards the SCs; the authors concluded that by exploiting the spatial transmit processing at massive-MIMO enabled MBSs, the interference at SC users can be significantly reduced. Therefore, accurate spatial modeling of the network nodes in such massive-MIMO equipped multi-tier HetNets has a pivotal role in the efficient design of interference mitigation techniques.

The spatial locations of the transmitter, receiver, interferers, and the scattering objects in a considered environment are critical factors in determining the performance of a wireless communication system [11, 12]. A primer on the fundamentals of spatial modeling based approaches for the analysis of network sum interference is presented in [13]. The knowledge of spatial locations of the interacting nodes determines the angular spread of the received signal, which can be quantified by using the theory of multipath shape factors originally proposed in [14] for two-dimensional (2-D) propagation environments, and then extended in [15, 16] to three-dimensional (3-D) radio propagation environments. These quantifiers in turn determine the second order fading statistics of the mobile radio channels such as the spatial autocovariance (SAC), coherence distance (CD), level-crossing-rate (LCR), and average-fade-duration (AFD). These parameters are of high interest in the design of efficient signal processing techniques, selection of appropriate error protection codes and interleaving schemes [17]. Therefore, it is essential to accurately model the network interference in the 3-D angular domain for the efficient design of communication systems and accurate prediction of the network performance. The work in [12] proposed a 2-D radio propagation model to characterize the network interference in the angular domain; the authors derived analytical expressions for the second order fading statistics of the signal-to-interference ratio (SIR). Although the simplification of a realistic propagation environment from 3-D to 2-D offers the advantage of mathematical tractability, it is of immense importance to model propagation channels in 3-D space for the emerging HetNet architectures that are envisioned to use large-scale planar antenna arrays at the MBSs and small coverage areas of their SCs coupled with BS heights that are significantly lower than that of surrounding building structures. For these reasons it is imperative to develop 3-D analytical models for characterizing the sum co-channel interference in the angular domain for HetNet architectures in emerging 5G communication networks.

This work addresses the aforementioned issues by proposing a 3-D model for characterizing the cumulative network interference in the angular domain for a two-tier HetNet with SCs in tier-1 overlaid with massive-MIMO enabled MBSs in tier-2. Analytical expressions are derived for characterization of second order fading statistics, such as the LCR, AFD, SAC, and CD of the desired signal, the interference signal, and the SIR. The proposed model is an extension of the model presented in [12] from a 2-D to a 3-D propagation scenario. Furthermore, our analytical results for second order fading statistics are derived for the Nakagami-m distributed signal envelopes that form a generalization of the results derived in [15] for Rayleigh distributed signal envelopes, which constitute a special case of our model. In addition, we also derive expressions for the joint characterization of the second order fading statistics with respect to the SIR.

The remainder of this paper is organized as follows. In Sec. II, the system model for the considered two-tier HetNet architecture is presented. In Sec. III, the analytical expressions for the LCR, AFD, SAC, and CD are derived for the desired signal, interference signal, and the SIR. In Sec. IV, a detailed analysis of the second-order fading statistics of the interference signal and SIR is presented along with a simulation-based validation of the derived expressions. Finally, the contributions of this paper are concluded in Sec. V.

II. SYSTEM MODEL

Consider the 3-D propagation scenario for a two-tier HetNet as shown in Fig. 1. The first tier is composed of multiple SCs served by low-cost remote radio units (RRUs) denoted by $\mathcal{T}_r^{\mathrm{SC}}$, overlaid by the massive-MIMO equipped MBSs denoted by $\mathcal{T}^{\mathrm{MC}}$ in the second tier. The subscript r is the index of the interfering small-cell BSs. The receiver $\mathcal{R}$ may be a single antenna user terminal or a highly mobile receiver equipped with an antenna array such as the receiver in a bus or train, which extends the network coverage to its passengers. The MBSs of the tier-2 support the high mobility users such as those in buses and trains as well as the cell-edge users of SCs. Both the tiers share the same spectrum in order to achieve a high spectral efficiency. However, the

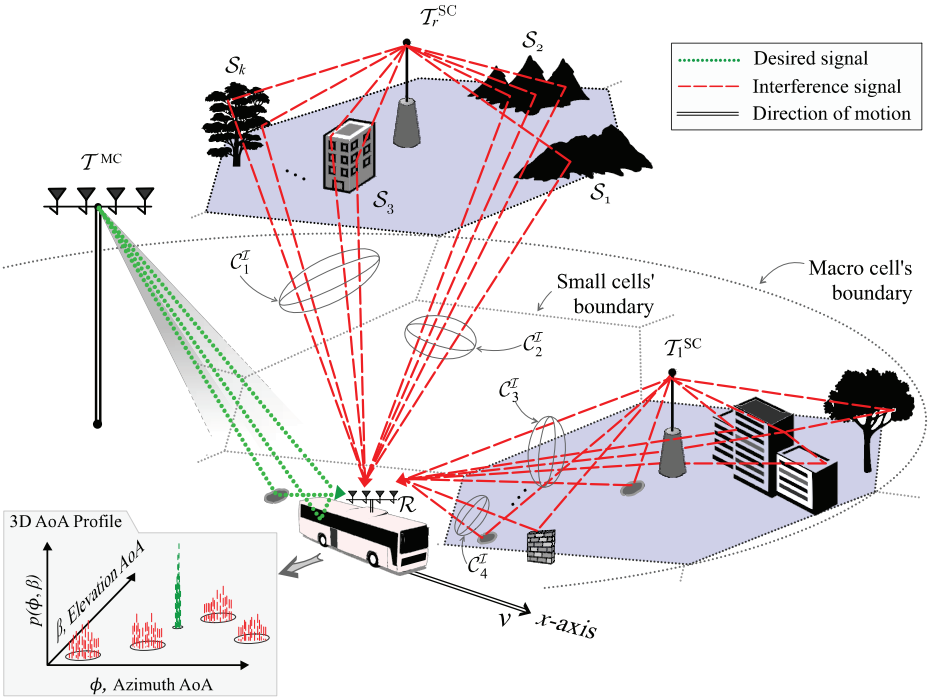

FIGURE 1: System Model.

transmissions from one tier may cause strong co-channel interference to the users in the other tier, which causes a performance bottleneck. By utilizing the direction-selective behavior of the interference power, this performance bottleneck can be alleviated. The desired multipath signals from the tier-2 MBS $\mathcal{T}^{\mathrm{MC}}$ to the receiver $\mathcal{R}$ are shown in Fig. 1 by dotted lines in green color, whereas the interfering multipath signals from the tier-1 SC BSs (and/or nearby SC users) are shown by dashed lines in red color in the same figure. Due to the simplicity in mathematical tractability and sufficiency of catering the important part of total signal energy, considering single-bounce has remained the first choice in geometry based channel modeling approaches [18, 19]. The considered model assumes a single bounce propagation mechanism in which each transmitted signal undergoes only one reflection or scattering from a certain k^{th} scattering object $\mathcal{S}_k$. Following the approach of [12] an equivalent interference network is assumed to replace the original multiple interfering sources, i.e., small cell BSs and user terminals are replaced with a single virtual interfering source $\mathcal{T}^{\mathcal{I}}$ as shown in Fig. 2 Each physical interferer $\mathcal{I}_k$ contributes to the interference signal at the receiver $\mathcal{R}$, where $1 \leq k \leq K$. These physical interferers are assumed to act as clustered scatterers at different spatial locations. For example the signals coming from high-rise buildings and or hills tend to exhibit a clustering behavior [18]. Moreover, the interferers may be multiple hotspots located nearby each other and/or densely populated user terminals tightly clustered together in a particular spatial region. These clusters of interferers have a Line-of-Sight (LoS) connection to both the transmitter and the receiver and are labeled as $\mathcal{C}_c^{\mathcal{I}}$, where the index in the subscript, $1 \leq c \leq C$, denotes a particular cluster. The physical interferers are assumed to be distributed over a wide geographic region independent from each other and clustered with respect to the geometry of tier-1 cells. The approximation of the interfering clusters in a particular propagation environment as some geometric shape such as a cylinder, spheroid, or an ellipsoid is based on the average behavior of irregularly scattered points over many realizations of the network. In this work, these clusters of physical interferers are assumed to be spheroidal regions with each spheroids radius and center position denoted by ρ_c and (x_c, y_c, z_c), respectively. Please refer to Fig. 3 for details. Let the direct LoS distance, transmitted power, azimuth angle-of-arrival (AoA), and elevation AoA associated with each physical interferer is denoted by d_k, P_k, ϕ_k, and β_k, respectively. The delay associated with each path is $\tau_k = \breve{\tau}_k + \rho_k/c$, where c is the speed of electromagnetic waves and $\breve{\tau}_k = \breve{\rho}_k/c$ is the propagation delay of the virtual backhaul path from $\mathcal{T}^{\mathcal{I}}$ to $\mathcal{I}_k$. The signals from these interfering radios are thus received as superimposed at the receiver $\mathcal{R}$.

A. DELAY AND DIRECTIONAL SPECTRUM

The joint delay and directional impulse response of the channel can be expressed as,

$$h_{\mathcal{I}}(\tau, \phi, \beta) = \sum_{k=1}^{K} h_{\mathcal{I},k}\delta(\tau - \tau_k)\delta(\phi - \phi_k)\delta(\beta - \beta_k), \quad (1)$$

where $h_{\mathcal{I},k} = \sqrt{\alpha_k P_k} d_k^{-n_{\mathrm{PL}}/2} \kappa_k \exp(j\theta_k)$ is the complex

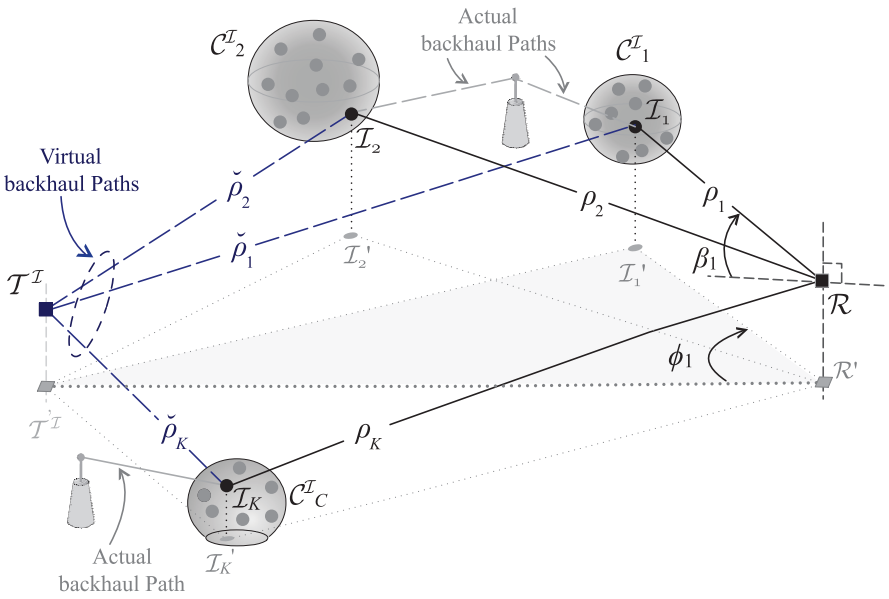

FIGURE 2: Illustration of physical interferer clusters represented by a virtual interfering source $\mathcal{T}^{\mathcal{I}}$. Details of the corresponding multipath links are also shown.

gain of k^{th} path. The power measured at distance of 1m away from k_{th} interferer is $\alpha_k P_k$. The parameters n_{PL} and $\kappa_k \exp(j\theta_k)$ represent the path loss exponent and fading experienced due to k^{th} interfering path, respectively. κ_k and θ_k are assumed to be independent and identically distributed (i.i.d.) for all the interferers. The interference delay directional spectrum (IDDS) can be expressed as,

$$\Xi_{\mathcal{I}-\text{DDS}}(\tau,\phi,\beta) = \sum_{k=1}^{K} |h_{\mathcal{I},k}|^2\, \delta(\tau-\tau_k)\delta(\phi-\phi_k)\delta(\beta-\beta_k). \tag{2}$$

This definition of IDDS is consistent with the definition of power azimuth-delay angular spectrum presented in [20]. From (2), the interference 3-D directional spectrum (IDiS) can be derived as,

$$\begin{aligned}\Xi_{\mathcal{I}-\text{DiS}}(\phi,\beta) &= \int_{\tau} \mathbb{E}\big[\Xi_{\mathcal{I}-\text{DDS}}(\tau,\phi,\beta)\big]\mathrm{d}\tau,\\ &\propto \int_{\tau} \mathbb{E}\big[|h_{\mathcal{I}}|^2|_{\tau,\phi,\beta}\big] f_{\tau,\phi,\beta}(\tau,\phi,\beta)\mathrm{d}\tau,\end{aligned} \tag{3}$$

where $\mathbb{E}[.]$ represents the expected value, $f_{\tau,\phi,\beta}(\tau,\phi,\beta)$ is the joint probability density function (pdf) of time-of-arrival (ToA), azimuth AoA, and elevation AoA. The expectation of power received from the k^{th} path is conditioned on its associated ToA, azimuth AoA, and elevation AoA, i.e., $\mathbb{E}\big[|h_I|^2|_{\tau,\phi,\beta}\big] = \mathbb{E}\big[|h_{I,k}|^2|_{\tau_k=\tau,\phi_k=\phi,\beta_k=\beta}\big]$. This joint definition of IDiS can be deduced to define interference azimuth spectrum (IAS) and interference elevation spectrum (IES), as follows:

$$\begin{aligned}\Xi_{\mathcal{I}-\text{AS}}(\phi) &= \int_{\beta} \mathbb{E}\big[\Xi_{\mathcal{I}-\text{DiS}}(\phi,\beta)\big]\mathrm{d}\beta,\\ &\propto \int_{\tau} \mathbb{E}\big[|h_{\mathcal{I}}|^2|_{\phi,\beta}\big] f_{\phi,\beta}(\phi,\beta)\mathrm{d}\beta,\end{aligned} \tag{4}$$

$$\begin{aligned}\Xi_{\mathcal{I}-\text{ES}}(\beta) &= \int_{\phi} \mathbb{E}\big[\Xi_{\mathcal{I}-\text{DiS}}(\phi,\beta)\big]\mathrm{d}\phi,\\ &\propto \int_{\tau} \mathbb{E}\big[|h_{\mathcal{I}}|^2|_{\phi,\beta}\big] f_{\phi,\beta}(\phi,\beta)\mathrm{d}\phi.\end{aligned} \tag{5}$$

where $f_{\phi,\beta}(\phi,\beta)$ is the joint pdf of azimuth and elevation AoA. The interfering objects close to the receiver draw the main features of interfering signal, therefore defining a threshold (p_e) on minimum significant power level of composite interference signal helps draw a spherical boundary of physical interferers around the receiver. Only the interferers within this bounding spheroid, with radius $\rho_e = p_e^{-1/n_{\text{PL}}}$ centered at the position of receiver, are the effective physical interferers. Spatial density function of interferers in a certain cluster of interferers c can be represented by $f^{(c)}_{x_{\mathcal{I}},y_{\mathcal{I}},z_{\mathcal{I}}}(x,y)$. This density function can be transformed from Cartesian to spherical representation as,

$$f^{(c)}_{\rho_{\mathcal{I}},\phi_{\mathcal{I}},\beta_{\mathcal{I}}}(\rho,\phi,\beta) = \frac{f^{(c)}_{x_{\mathcal{I}},y_{\mathcal{I}},z_{\mathcal{I}}}(x,y,z)}{|J(x,y,z)|}\Bigg|_{\substack{x=\rho\cos\beta\sin\phi,\\ y=\rho\cos\beta\cos\phi,\\ z=\rho\sin\beta,}} \tag{6}$$

where the Jacobian transformation can be expressed in simplified form as $J(x,y,z) = 1/\rho^2\cos\beta$. After integrating (6) over the radial distance ρ, we get the joint pdf of AoA for the

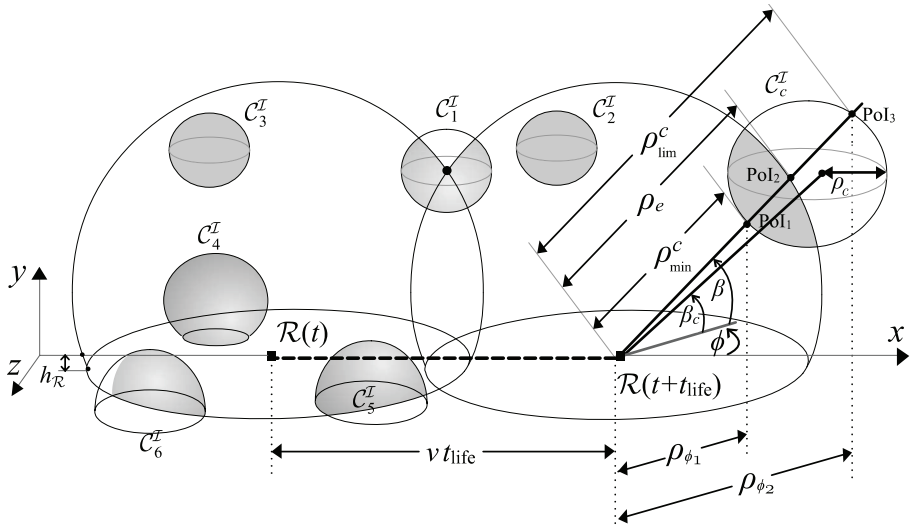

FIGURE 3: Geometric composition of included and excluded interferers.

interferers in cluster c, which can be expressed in simplified form as,

$$f^{(c)}_{\phi_{\mathcal{I}},\beta_{\mathcal{I}}}(\phi,\beta)=\int_{\rho^{(c)}_{\min}}^{\rho^{(c)}_{\max}}\rho^2\cos\beta\, f^{(c)}_{x_{\mathcal{I}},y_{\mathcal{I}},z_{\mathcal{I}}}(x,y,z)\,\mathrm{d}\rho, \quad (7)$$

where $\rho^{(c)}_{\min}$ and $\rho^{(c)}_{\max}$ is the distance from the receiver to the nearest and farthest interferer in a given particular direction (i.e., given ϕ and β) for a certain cluster c. These distances can be obtained as,

$$\left.\begin{matrix}\breve{\rho}^{(c)}_{\max}\\ \rho^{(c)}_{\min}\end{matrix}\right\}=z_c\sin\beta+\cos\beta(y_c\cos\phi+x_c\sin\phi)\pm\Big(\rho_c^2-x_c^2-y_c^2-z_c^2+(y_c\cos\beta\cos\phi+z_c\sin\beta+x_c\cos\beta\sin\phi)^2\Big)^{1/2}. \quad (8)$$

The distance of farther scatterers is determined by the overlap scenario of the interferers cluster with the bounding spheroid; as it is limited by the bounding spheroid, see the points of intersection (PoI) in Fig 3. Therefore, it takes value as, $\rho^{(c)}_{\max}=\min\left(\rho_e,\breve{\rho}^{(c)}_{\max}\right)$. The interferers in each cluster may follow a certain spatial distribution (Gaussian, uniform, or parabolic, etc). Assuming the interferers uniformly distributed within each cluster, the interferers spatial density function can be expressed as,

$$f^{(c)}_{x_{\mathcal{I}},y_{\mathcal{I}},z_{\mathcal{I}}}(x,y,z)=\begin{cases}\dfrac{1}{V^{(c)}} & ;\ (x,y,z)\in\text{effecitve portion of the interferers' cluster } c,\\ 0 & ;\ \text{otherwise,}\end{cases} \quad (9)$$

where the volume $V^{(c)}$ of effective region of interferers' cluster c can be expressed as,

$$V^{(c)}=\begin{cases}\dfrac{4}{3}\pi\rho_c^3 & ;\sqrt{x_c^2+y_c^2+z_c^2}\le(\rho_e-\rho_c),\\ \dfrac{\pi(-d_e+\rho_c+\rho_e)^2}{12d_e}\Big(d_e^2-3\times(\rho_c-\rho_e)^2+2d_e(\rho_c+\rho_e)\Big) & ;\ \text{otherwise,}\end{cases} \quad (10)$$

where the separation distance of the cluster's center from the receiver's current position is $d_e=\sqrt{(x_{\mathcal{R}}-x_c)^2+(y_{\mathcal{R}}-y_c)^2+(z_{\mathcal{R}}-z_c)^2}$. For the considered equivalent network model with an introduced virtual source in Fig. 2, when the delay of virtual backhaul paths $\breve{\tau}$ is assumed i.i.d. and the speed of electromagnetic waves c being a constant value independent of spatial location of interferers, the joint ToA and AoA density function in (3) can be replaced as $f(\tau,\phi,\beta)\propto f(\breve{\tau})f(\rho,\phi,\beta)$. Furthermore, the power of interference signal associated to a path with length ρ can be given as $\mathbb{E}\big[|h_{\mathcal{I}}|^2|_{\tau,\phi,\beta}\big]\propto\rho^{-n_{\text{PL}}}$. Closed-form analytical relationship for IDiS for all the interfering clusters can be obtained from (3), as follows,

$$\begin{aligned}\Xi_{\mathcal{I}-\text{DiS}}(\phi,\beta)&\propto\mathcal{N}\sum_{c=1}^{C}\int_{\rho^{(c)}_{\min}}^{\rho^{(c)}_{\max}}\rho^{-n_{\text{PL}}}f^{(c)}_{\rho_{\mathcal{I}},\phi_{\mathcal{I}},\beta_{\mathcal{I}}}(\rho,\phi,\beta)\mathrm{d}\rho\times\int_0^{\infty}f^{(c)}_{\breve{\tau}_{\mathcal{I}}}(\breve{\tau})\mathrm{d}\breve{\tau},\\&=\mathcal{N}\sum_{c=1}^{C}\frac{\cos\beta}{V^{(c)}}\int_{\rho^{(c)}_{\min}}^{\rho^{(c)}_{\max}}\rho^{2-n_{\text{PL}}}\mathrm{d}\rho,\\&=\mathcal{N}\sum_{c=1}^{C}\frac{\cos\beta\,\left(\rho^{(c)}_{\max}-\rho^{(c)}_{\min}\right)^{3-n_{\text{PL}}}}{(3-n_{\text{PL}})V^{(c)}},\end{aligned} \quad (11)$$

where $\mathcal{N}$ is a normalization constant such that $\iint\Xi^{\text{IDS}}(\phi,\beta)\,\mathrm{d}\beta\mathrm{d}\phi=1$. For the desired signal arriving at the receiver $\mathcal{R}$ from the MBS $\mathcal{T}^{\text{MC}}$ via the scattering points $\mathcal{S}_p$, the joint density function for ToA, azimuth AoA, and elevation AoA can be obtained through the following transformation,

$$f_{\tau_{\rm S},\phi_{\rm S},\beta_{\rm S}}(\tau,\phi,\beta)=\frac{f_{\rho_{\mathcal{S}},\phi_{\rm S},\beta_{\rm S}}(\rho,\phi,\beta)}{|J(\rho,\phi,\beta)|}\Bigg|_{\substack{\rho=\frac{1}{2}(c^2\tau^2-x_{\rm M}^2\\ -y_{\rm M}^2-z_{\rm M}^2)\left(c\tau\right.\\ \left.-\sqrt{x_{\rm M}^2+y_{\rm M}^2}\cos\beta\right.\\ \left.\times\cos\phi+z_{\rm M}\sin\beta\right)^{-1}}},\tag{12}$$

where $x_{\rm M}$, $y_{\rm M}$, and $z_{\rm M}$ are the coordinates of MBS w.r.t. the origin assumed at the location of receiver. The radial parameter ρ, represents the distance of receiver from a scattering point. Substituting this in an expression written for the desired signals similar to (2) (instead of interference signals), we get the signal DDS. Which can further be extended to define the signal DS. The simplified solution is expressed can be obtained as

$$\begin{aligned}\Xi_{\mathcal{S}-\rm DiS}(\phi,\beta)\propto&\\ \mathcal{N}\int_{\tau_{\min}}^{\tau_{\max}}&\frac{(c\tau)^{-n_{\rm PL}}c\cos\beta f_{x_{\mathcal{S}},y_{\rm S},z_{\rm S}}(x,y,z)}{8(\sqrt{x_{\rm M}^2+y_{\rm M}^2}\cos\beta\cos\phi-c\tau+z_{\rm M}\sin\beta)^4}\\ &\times(x_{\rm M}^2+y_{\rm M}^2+z_{\rm M}^2-c^2\tau^2)^2\Big(x_{\rm M}^2+y_{\rm M}^2+z_{\rm M}^2+c^2\tau^2\\ &-2c\tau\left(\sqrt{x_{\rm M}^2+y_{\rm M}^2}\cos\beta\cos\phi+z_{\rm M}\sin\beta\right)\Big){\rm d}\tau,\end{aligned}\tag{13}$$

where the direction dependant limits on τ can be calculated as,

$$\begin{aligned}\tau_{\rm i}=\frac{1}{c}\Bigg\{&\rho_{\rm i}+\Big\{\rho_{\rm i}^2+x_{\rm M}^2+y_{\rm M}^2+z_{\rm M}^2-2\rho_{\rm i}\\ &\times\left(\sqrt{x_{\rm M}^2+y_{\rm M}^2}\cos\beta_m\cos\phi_m+z_{\rm M}\sin\beta_m\right)\Big\}^{1/2}\Bigg\},\end{aligned}\tag{14}$$

where ${\rm i}\in\{\min,\max\}$. The parameters $\rho_{\min}$ and $\rho_{\max}$ represent the distance of nearest and farthest scattering point from the receiver for a fixed direction of observation. These distances are dependant on the geometry of scattering volume's shape. For the desired multipath signals arriving from MBS to the receiver via different scattering points, the geometry of scattering region may be significantly different from the geometry of interfering clusters. The high elevation of MBS compared to the scattering structures in its vicinity makes the BS side of the link a scattering free region. Only the scattering objects in the vicinity of the receiver at the ground correspond in the arrival of signals. In such scenario, when ignoring the antenna beam patterns, it is reasonable to assume the pdf of AoA observed at the receiver as uniformly distributed over the whole angular span (i.e., a spherical shaped scattering volume with its center at the receiver). For the scenarios, when the MBS is equipped with highly directional antenna (e.g., mmMIMO based BS), causes truncation of spatial scattering region leading to the pdf of AoA observed at the receiver deviate from uniformly distribution to other distributions. For macro-cellular environments, various studies for the effect of directional antennas employed at BS on the pdf of ToA and AoA are presented in the literature, see e.g., [21–23]. The direction dependant limits ($\tau_{\max}$, $\tau_{\min}$) can thus be taken as derived in [22, 24]. Further, the signal AS and ES can thus be defined as

$$\Xi_{\mathcal{S}}^{\rm SAS}(\phi)=\int_{\beta_{\rm span}}\int_{\tau_{\rm span}}\rho^{-n_{\rm PL}}f_{\tau_{\mathcal{S}},\phi_{\mathcal{S}},\beta_{\mathcal{S}}}(\tau,\phi,\beta){\rm d}\tau{\rm d}\beta.\tag{15}$$

$$\Xi_{\mathcal{S}}^{\rm SES}(\beta)=\int_{\phi_{\rm span}}\int_{\tau_{\rm span}}\rho^{-n_{\rm PL}}f_{\tau_{\mathcal{S}},\phi_{\mathcal{S}},\beta_{\mathcal{S}}}(\tau,\phi,\beta){\rm d}\tau{\rm d}\phi.\tag{16}$$

The joint and marginal pdfs of ToA and AoA can be obtained for semi-spheroidal spatial channel model proposed in [22] and [24] for uniform and Gaussian distributed scattering objects, respectively. Poisson Point Process (PPP) is widely used for placement of nodes in a wireless network, the position of centers of the interferers' clusters can be drawn within the defined 3-D spatial region. The amount of clusters can be drawn from Poisson distribution within an arbitrary region as,

$$p(\mathcal{C})=\frac{\exp(-\mu)\mu^{\mathcal{C}}}{\mathcal{C}!},\tag{17}$$

where $\mu=\lambda_{\mathcal{C}}\mathcal{V}$; where $\lambda_{\mathcal{C}}$ and $\mathcal{V}$ represent the density of cluster centers and the volume of effective region, respectively. A realization of the network for $\lambda_{\mathcal{C}}=0.02$ is plotted in Fig. 4, where the effective scattering points from three different time instances (i.e., $t=0$sec, $t=30$sec, and $t=60$sec) are highlighted. The radius of clusters ρ_c is drawn from uniform distribution in the range, $70{\rm m}\leq\rho_c\leq120{\rm m}$. The position of interferers within a cluster (spheroid) are drawn from homogeneous PPP with an intensity $\lambda_{\mathcal{I}}=0.02$ and the radius of effective interferers bounding spheroid is taken as $\rho_e=300$m. The mobility of receiver $\mathcal{R}$ moving with velocity v in a particular direction imposes time variability in the channel characteristics. With the mobility of receiver, some interfering cluster move in and some move out of the bounding spheroid associated with minimum effective interference power threshold; therefore, it is of vital importance to discuss the lifespan associated with each cluster.

B. LIFESPAN OF INTERFERING CLUSTERS

For simplicity of mathematical expressions, the $x-$ axis of the coordinates system is assumed along the direction of MS's motion. A cluster stays effective until its (instantaneous) LoS distance from the receiver stays below the threshold ρ_e. The lifespan $t_{\rm life}$ of a certain cluster, e.g., $\mathcal{C}_1$ in Fig. 3, can be calculated by using basic trigonometry. The horizontal distance between the positions $\mathcal{R}(t)$ and $\mathcal{R}(t+t_{\rm life})$, can be expressed as, $2\sqrt{\rho_e^2-y_1^2-z_1^2}$. The lifespan of cluster $\mathcal{C}_1^{\mathcal{I}}$ is thus given by $t_{\rm life}=2\sqrt{\rho_e^2-y_1^2-z_1^2}/v$. The cumulative distribution function (cdf) of $t_{\rm life}$ can be obtained by extending the approach adopted in [12] from its definition in 2-D to 3-D space; it can be expressed as,

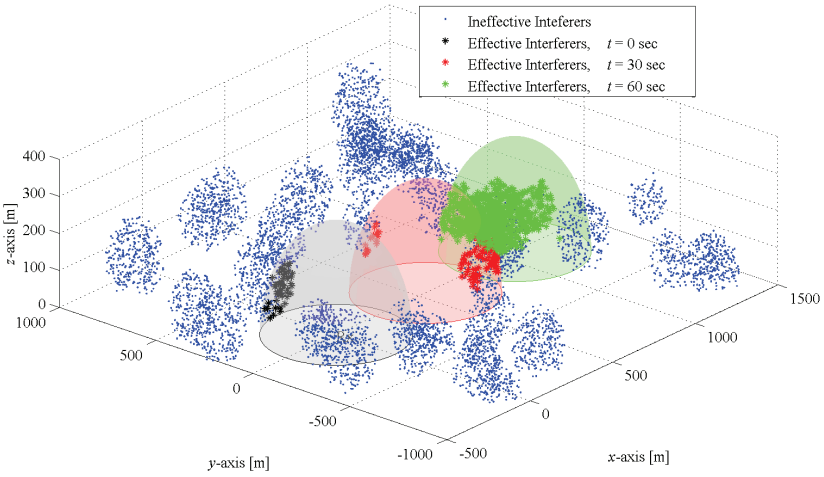

FIGURE 4: Spatial evolution of the effective interferer cluster in one simulation run.

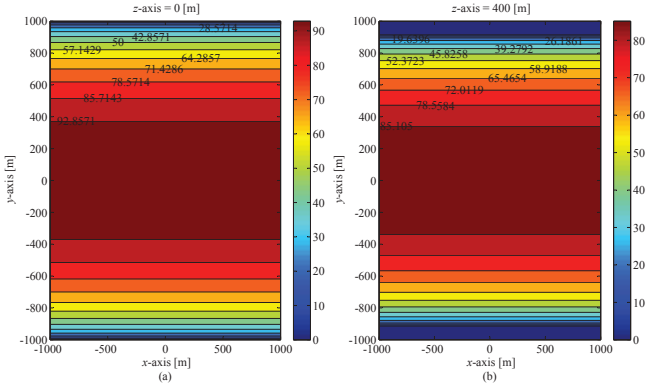

FIGURE 5: Contours of interfering cluster's lifespan for different altitudes, z: (a) $z = 0$ m, and (b) $z = 400$ m.

$$F_{t_{\text{life}}}(t_{\text{life}}) = \iiint f_{x_c,y_c,z_c}(x,y,z)\mathrm{d}x\mathrm{d}y\mathrm{d}z, \qquad (18)$$

where $f_{x_c,y_c,z_c}(x,y,z)$ is the pdf of the spatial position of clusters' center on the entire considered region. The integration in (18) only holds for the region when the condition, $t_{\text{life}} \geq 2\sqrt{r_{\text{eff}}^2 - y^2 - z^2}/v_R$, is satisfied. The average lifespan of interference clusters can be calculated as,

$$\mathbb{E}[t_{\text{life}}] = \iiint \frac{2\sqrt{\rho_e^2 - y^2 - z^2}}{v} f_{x_c,y_c,z_c}(x,y,z)\mathrm{d}x\mathrm{d}y\mathrm{d}z. \qquad (19)$$

Lifespan of an interfering cluster is plotted in Fig. 5, where the receiver is considered moving at a velocity of $v = 20$m/s, the radius of bounding spheroid as $\rho_e = 1$km. The lifespan of a cluster w.r.t. different vertical positions of its center is plotted in Fig. 5 (a) and (b), for elevations of 0m and 400m, respectively. It is evident that the lifespan associated to a certain cluster has a high value for its positions closer to the trajectory of receiver's mobility. Moreover, the significance of considering the elevation plane into consideration for accurately modeling the network interference is also clearly evident.

III. SECOND ORDER FADING STATISTICS OF DESIRED AND INTERFERENCE SIGNALS

The directional statistics of the desired and interference signals can help in characterization of random fluctuations in the received signal. In various propagation scenarios, different distributions are considered as appropriate to model the the envelope R of received signal, e.g., Rayleigh distribution is widely used. Various superimposed i.i.d. Rayleigh fading signals follow a Nakagami-m distributed amplitude [25]. The power of a composite interference signal from multiple interference sources has often been modeled as Gamma distributed [11]; which further suggests that the amplitude of interference signal (if defined as proportional to square root of the power) is Nakagami-m distributed. Nakagami-m distribution also offers several advantages in terms of ease in mathematical interpretability and generalization to deduce various other widely used distributions, e.g., Rayleigh distribution can be deduced from Nakagami-m distribution as a special case. These reasons are the motivation to model the envelopes of received interference signal as Nakagami-m distributed. The pdf of Nakagami-m distribution can be expressed as,

$$f_R(r) = \frac{2m^m r^{2m-1}}{\Gamma(m)P_T^m} \exp\left(\frac{-mr^2}{P_T}\right), \quad r \geq 0 \text{ and } m \geq \frac{1}{2}, \qquad (20)$$

where $P_T = \mathbb{E}[r^2]$ is the average total received power in the local area, $\Gamma(.)$ is the Gamma function, and $m = \mathbb{E}[r^2]/\text{var}(r^2)$ is the shape parameter.

A. NOTABLE 3-D ANGULAR SPREAD QUANTIFIERS

To measure the dispersion of energy in angular domain, various quantifiers have been proposed in the literature, see

TABLE 1: Three-dimensional Multipath Shape Factors Proposed in [15]

Quantifier	Mathematical Expression	Range	Description
Angular Spread	$\Upsilon = \sqrt{1 - \frac{S_1^{0\,2} + \lvert S_1^1 \rvert^2}{S_0^{0\,2}}}$	$0 \sim 1$	0 indicates the signal arriving from exactly one single azimuthal direction; 1 indicates no clear bias
Elevational Constriction	$\xi = \frac{\frac{3}{2} S_2^0 S_0^0 - \left(S_1^{0\,2} + \frac{1}{2}\lvert S_1^1 \rvert^2\right)}{S_0^{0\,2} - \left(S_1^{0\,2} + \lvert S_1^1 \rvert^2\right)}$	$-0.5 \sim 1$	-0.5 shows the received signal's high concentration along a single elevational cone; 1 shows signal arriving from two opposite elevation angles at same azimuth angle.
45°-Inclined Constriction	$\chi = \frac{2\lvert S_2^1 S_0^0 - S_1^0 S_1^1 \rvert}{S_0^{0\,2} - \left(S_1^{0\,2} + \lvert S_1^1 \rvert^2\right)}$	$0 \sim 1$	0 denotes mirror symmetry along horizontal and/or vertical axes; 1 denotes the arrival of exactly two paths in vertical axis from mirror symmetric directions relative to a 45°-inclined axis
Azimuthal Constriction	$\zeta = \frac{\lvert S_2^2 S_0^0 - S_1^{1\,2} \rvert}{S_0^{0\,2} - \left(S_1^{0\,2} + \lvert S_1^1 \rvert^2\right)}$	$0 \sim 1$	1 denotes exactly two multipaths arriving from same elevation; 0 denotes no bias
Azimuth of Maximum Fading at 45° Elevation	$\phi_{\beta 45}^{\max} = \arg\left\{S_2^1 S_0^0 - S_1^0 S_1^1\right\}$	$0 \sim 2\pi$	Indicates the azimuth angle, at a fixed elevation of 45°, causing maximum fading.
Azimuth of Maximum Fading at 0° Elevation	$\phi_{\beta 0}^{\max} = \frac{1}{2}\arg\left\{S_2^2 S_0^0 - S_1^{1\,2}\right\}$	$0 \sim \pi$	Indicates the exact azimuth angle, at a fixed elevation of 0°, causing maximum fading.

e.g., [14] and [15, 16] for quantifiers in 2-D and 3-D spatial domains, respectively. We have adopted the 3-D multipath shape factors presented in [15] for quantification of energy in 3-D angular domain. For convenience of the readers, these quantifiers are presented in Table 1. The harmonic coefficients S_n^m used in the definition of shape factors can be computed as,

$$
\begin{aligned}
S_0^0 &= \iint f(\phi,\beta)\cos\beta \,\mathrm{d}\beta\mathrm{d}\phi,\\
S_1^0 &= \iint f(\phi,\beta)\sin\beta\cos\beta \,\mathrm{d}\beta\mathrm{d}\phi,\\
S_1^1 &= \iint f(\phi,\beta)\cos^2\beta e^{j\phi} \,\mathrm{d}\beta\mathrm{d}\phi,\\
S_2^0 &= \iint f(\phi,\beta)\left(\sin^2\beta - \frac{1}{3}\right)\cos\beta \,\mathrm{d}\beta\mathrm{d}\phi,\\
S_2^1 &= \iint f(\phi,\beta)\cos^2\beta\sin\beta e^{j\phi} \,\mathrm{d}\beta\mathrm{d}\phi,\\
S_2^2 &= \iint f(\phi,\beta)\cos^3\beta e^{j2\phi} \,\mathrm{d}\beta\mathrm{d}\phi.
\end{aligned}
$$

B. LEVEL CROSSING RATE

The LCR, N_R, is defined as the average number of crossings per unit time (or distance) that a signal drops below a given threshold level R. The LCR can be expressed, as follows,

$$
N_R = \int_0^\infty \dot{r} f_{r,\dot{r}}(r = R, \dot{r})\mathrm{d}\dot{r}, \tag{21}
$$

where $f_{r,\dot{r}}(r = R, \dot{r})$ is the joint pdf of envelope and its derivative. An expression for LCR can be derived for Nakagami-m distributed envelope in the context of 3-D radio propagation scenario, by extending the definition presented in [15] for Rayleigh distributed envelope. The derived LCR expression in terms of 3-D multipath shape factors for Nakagami-m distributed envelope is presented as below,

$$
\begin{aligned}
N_{R_{(.)}} = \frac{\omega_D \Upsilon_{(.)} \tilde{R}_{(.)}^{\left(2m_{(.)}-1\right)} m_{(.)}^{\left(m_{(.)}-1/2\right)} \exp\left(-m_{(.)}\tilde{R}_{(.)}^2\right)}{\sqrt{3\pi}\Gamma(m_{(.)})}\\
\times\left\{1 + \frac{3}{2}\left(\xi_{(.)}\left(2\sin^2\beta_v - \frac{2}{3}\right) + \chi_{(.)}\sin(2\beta_v)\right.\right.\\
\left.\times\cos(\phi_v - \phi_{\beta 45_{(.)}}^{\max}) + \zeta_{(.)}\cos^2\beta_v\right.\\
\left.\left.\times\cos\left(2(\phi_v - \phi_{\beta 0_{(.)}}^{\max})\right)\right)\right\}^{\frac{1}{2}},
\end{aligned}
\tag{22}
$$

where ω_D is the maximum Doppler angular frequency offset, ϕ_v is the azimuth direction of receiver's motion, β_v is the elevation direction of receiver's motion, and $\tilde{R}_{(.)}$ is the normalized threshold as $\tilde{R}_{(.)} = R_{(.)}/P_{(.)}$. This expression for LCR ($N_{R_{(.)}}$) can be used to independently characterize the LCR of interference and desired signals as $N_{R_\mathcal{I}}$ and $N_{R_\mathcal{S}}$, by using the appropriate set of shape factors calculated from joint pdf of AoA for interference and desired signals, respectively. Along the significance of independently characterized LCR for interference and desired signals, it is also of high significance to study it for SIR (η) to characterize the behaviour of composite received signal in a 3-D radio propagation environment of HetNets. In this regard, a joint pdf of envelopes and their slopes for both interference and desired signals, i.e., $f_{r_\mathcal{I},\dot{r}_\mathcal{I},r_\mathcal{S},\dot{r}_\mathcal{S}}(r_\mathcal{I},\dot{r}_\mathcal{I},r_\mathcal{S},\dot{r}_\mathcal{S})$, is required at any spatial position. The threshold level of observation for characterizing N_{R_η} is defined as $R_\eta = r_\mathcal{I}^2/r_\mathcal{S}^2$. Interpreting the analogy between the mathematical relationship derived in [12] for LCR of SIR in a 2-D propagation environment for Nakagami-m distributed envelope and the relationship derived in [15] for LCR of signal in 3-D propagation environment for Rayleigh distributed envelope, a relationship can be derived directly for LCR of SIR in a 3-D propagation environment with Nakagami-m distributed envelope. When the interference and desired signal channels are assumed independent, the LCR of SIR given in [12], is presented as follows,

$$N_{R_\eta} = \int_0^\infty f_{r_\mathcal{I}}(r_\mathcal{I})\, f_{r_\mathcal{S}}\left(\sqrt{\tilde{R}_\eta r_\mathcal{I}^2}\right) \mathrm{d}r_\mathcal{I} \times \int_{-\infty}^{\infty}\int_{-\infty}^{\dot{r}_\mathcal{I}} \frac{\sqrt{\tilde{R}_\eta}}{\min\left\{|1/\dot{r}_\mathcal{I}|, |\sqrt{\tilde{R}_\eta}/\dot{r}_\mathcal{S}|\right\}} f_{\dot{r}_\mathcal{I}}(\dot{r}_\mathcal{I}) f_{\dot{r}_\mathcal{S}}(\dot{r}_\mathcal{S}) \mathrm{d}\dot{r}_\mathcal{I} \mathrm{d}\dot{r}_\mathcal{S}, \tag{23}$$

where the pdf of $r_\mathcal{S}$ and $r_\mathcal{I}$ follow Nakagami-m distribution, as given in (20); whereas, the pdf of their slopes $\dot{r}_\mathcal{S}$ and $\dot{r}_\mathcal{I}$ follow Gaussian distribution [26] with variance $\sigma^2_{V_\mathcal{S}}/(2m_\mathcal{S})$ and $\sigma^2_{V_\mathcal{I}}/(2m_\mathcal{I})$, respectively. The fading rate variance of complex received voltage of interference $\sigma^2_{V_\mathcal{I}}$ and desired $\sigma^2_{V_\mathcal{S}}$ signals, as a function of 3-D multipath shape factors in [15], is given as follows,

$$\sigma^2_{V_{(.)}} = \frac{\omega_D^2 \Upsilon^2_{(.)} P_{(.)}}{3}\left\{1 + \frac{3}{2}\left(\xi_{(.)}\left(2\sin^2\beta_v - \frac{2}{3}\right) + \chi_{(.)}\sin(2\beta_v)\cos\left(\phi_v - \phi^{\max}_{\beta 45_{(.)}}\right) + \zeta_{(.)} \times \cos^2\beta_v \cos\left(2(\phi_v - \phi^{\max}_{\beta 0_{(.)}})\right)\right)\right\}. \tag{24}$$

Following the same approach as used in [12] for the case of 2-D propagation environment, simplified expressions for N_{R_η} in a 3-D propagation scenario can be derived for two special cases.

Case-I

An analytical expression for the LCR of SIR can be derived for the case when rate of fluctuations in the interference signal is much slower than it is in the desired signal, i.e., $N_{R_\mathcal{I}} \ll N_{R_\mathcal{S}}$. Given, the threshold level is taken the same for both interference and desired signals, and it satisfies $\tilde{R}_\eta = \tilde{R}^2_\mathcal{S} P_\mathcal{S}/r^2_\mathcal{I}$, the simplified expression for LCR of SIR can be written as,

$$N_{R_\eta} = \int_0^\infty \frac{2\omega_D \Upsilon_\mathcal{S}\left(\frac{\tilde{R}_\eta r^2_\mathcal{I}}{P_\mathcal{S}}\right)^{m_\mathcal{S}-\frac{1}{2}} m_\mathcal{I}^{m_\mathcal{I}} m_\mathcal{S}^{m_\mathcal{S}-\frac{1}{2}} r_\mathcal{I}^{2m_\mathcal{I}-1}}{\sqrt{3\pi}\Gamma(m_\mathcal{S})\Gamma(m_\mathcal{I}) P_\mathcal{I}^{m_\mathcal{I}}} \times \exp\left(-\frac{m_\mathcal{S}\tilde{R}_\eta r^2_\mathcal{I}}{P_\mathcal{S}} - \frac{m_\mathcal{I} r^2_\mathcal{I}}{P_\mathcal{I}}\right)\left\{1 + \frac{3}{2}\left(\xi_\mathcal{S}\left(2\sin^2\beta_v - \frac{2}{3}\right) + \chi_\mathcal{S}\sin(2\beta_v)\cos(\phi_v - \phi^{\max}_{\beta 45}) + \zeta_\mathcal{S}\cos^2\beta_v \cos\left(2(\phi_v - \phi^{\max}_{\beta 0})\right)\right)\right\}^{\frac{1}{2}} \mathrm{d}r_\mathcal{I}, \tag{25}$$

Case-II

For the case when rate of fluctuations in the interference signal is much faster than it is in the desired signal, i.e., $N_{R_\mathcal{I}} \gg N_{R_\mathcal{S}}$, expression for LCR of SIR can be expressed as,

$$N_{R_\eta} = \int_0^\infty \frac{2\omega_D \Upsilon_\mathcal{I}\left(\frac{r^2_\mathcal{S}}{\tilde{R}_\eta P_\mathcal{I}}\right)^{m_\mathcal{I}-\frac{1}{2}} m_\mathcal{I}^{m_\mathcal{I}-\frac{1}{2}} m_\mathcal{S}^{m_\mathcal{S}} r_\mathcal{S}^{2m_\mathcal{S}-1}}{\sqrt{3\pi}\Gamma(m_\mathcal{I})\Gamma(m_\mathcal{S}) P_\mathcal{S}^{m_\mathcal{S}}} \times \exp\left(-\frac{m_\mathcal{I} r^2_\mathcal{S}}{\tilde{R}_\eta P_\mathcal{I}} - \frac{m_\mathcal{S} r^2_\mathcal{S}}{P_\mathcal{S}}\right)\left\{1 + \frac{3}{2}\left(\xi_\mathcal{I}\left(2\sin^2\beta_v - \frac{2}{3}\right) + \chi_\mathcal{I}\sin(2\beta_v)\cos(\phi_v - \phi^{\max}_{\beta 45}) + \zeta_\mathcal{I}\cos^2\beta_v \cos\left(2(\phi_v - \phi^{\max}_{\beta 0})\right)\right)\right\}^{\frac{1}{2}} \mathrm{d}r_\mathcal{S}, \tag{26}$$

C. AVERAGE FADE DURATION

AFD is the average duration for with the envelope of received signal stays below a given threshold level. The AFD can be calculated by tracking the the total time a signal stays below the threshold level divided by the total number of crossings, i.e., $\tau_R = \mathrm{Prob}(r \leq R)/N_R$. This suggests that,

$$\bar{\tau}_R = \frac{1}{N_R}\int_0^R f_r(r)\mathrm{d}r. \tag{27}$$

After substituting the expression derived for LCR (22) and the pdf of received signal's envelope (20) into (27); the simplified solution can be expressed as,

$$\bar{\tau}_{R_{(.)}} = \frac{\sqrt{3\pi}\left(\Gamma(m_{(.)}) - \hat{\Gamma}\left(m_{(.)}, \frac{m_{(.)}\tilde{R}^2_{(.)}}{P_{(.)}}\right)\right)}{\omega_D \Upsilon_{(.)} \tilde{R}^{(2m_{(.)}-1)}_{(.)} m^{(m_{(.)}-1/2)}_{(.)} \exp\left(-m_{(.)}\tilde{R}^2_{(.)}\right)}\left\{1 + \frac{3}{2} \times \left(\xi_{(.)}\left(2\sin^2\beta_v - \frac{2}{3}\right) + \chi_{(.)}\cos(\phi_v - \phi^{\max}_{\beta 45_{(.)}}) \times \sin(2\beta_v) + \zeta_{(.)}\cos^2\beta_v \cos\left(2(\phi_v - \phi^{\max}_{\beta 0_{(.)}})\right)\right)\right\}^{-\frac{1}{2}}, \tag{28}$$

where $\hat{\Gamma}(.,.)$ is the incomplete Gamma function. This relationship for AFD ($\bar{\tau}_{R_{(.)}}$) can be used independently to characterize both the interference ($\bar{\tau}_{R_\mathcal{I}}$) and desired signal ($\bar{\tau}_{R_\mathcal{S}}$) by substituting their respective set of shape factors. Further, by following (27) and the approach used in [12] for the case of 2-D propagation scenario, an expression for AFD can be derived to characterize the SIR. Simplified solution for AFD of SIR can be expressed as,

$$\bar{\tau}_{R_\eta} = \frac{1}{N_{R_\eta}} I_{\frac{m_{\mathcal{S}}\bar{R}_\eta}{m_{\mathcal{S}}\bar{R}_\eta + m_{\mathcal{I}}}}(m_{\mathcal{S}}, m_{\mathcal{I}}) \tag{29}$$

$I_{(.)}(.,.)$ is the regularized incomplete Beta function. The LCR of SIR N_{R_η} in (29) can be substituted from (23). Moreover, mathematical expression of AFD for two special cases, as discussed for LCR, can be obtained by using the corresponding expression of N_{R_η} from (26) or (26) for case-I and case-II, respectively.

D. ENVELOPE CORRELATION APPROXIMATION

The SAC of received signal envelope is regarded as an important second-order statistic. This calculates the correlation of envelops as function change in receiver's position (i.e., l) along a certain direction of receivers motion (i.e., ϕ_v and β_v).

$$\varrho_{(.)}(l, \phi_v, \beta_v) = \frac{\mathbb{E}\left[\Theta_{(.)}(l)\right] - \mathbb{E}^2\left[r_{(.)}\right]}{\mathbb{E}\left[r_{(.)}^2\right] - \mathbb{E}^2\left[r_{(.)}\right]} \tag{30}$$

where $\Theta_{(.)}(l) = r_{(.)}\{\vec{\mathrm{l}}_0\} r_{(.)}\{\vec{\mathrm{l}}_0 + l\hat{\mathrm{l}}\}$. $\vec{\mathrm{l}}_0$ and $\hat{\mathrm{l}}$ represents the reference position of the receiver and unit vector pointing towards the direction of receiver's motion in 3-D space, respectively. By extending the approach presented in [14] from Rayleigh to Nakagami-m distribution, and using three-dimensional shape factors presented in [15], the simplified solution for envelope correlation function can be obtained as,

$$\begin{aligned}\varrho_{(.)}(l, \phi_v, \beta_v) \approx \\ \exp\left\{\frac{-\Upsilon_{(.)}^2 m_{(.)} \Gamma^2(m_{(.)})}{3\left(m_{(.)}\Gamma^2(m_{(.)}) - \Gamma^2(m_{(.)} + \frac{1}{2})\right)}\left[1 + \frac{3}{2}\left(\xi_{(.)}\right.\right.\right. \\ \times\left(2\sin^2\beta_v - \frac{2}{3}\right) + \chi_{(.)}\sin(2\beta_v)\cos\left(\phi_v - \phi_{\beta 45_{(.)}}^{\max}\right) \\ \left.\left.\left. + \zeta_{(.)}\cos^2\beta_v \cos\left(2(\phi_v - \phi_{\beta 0_{(.)}}^{\max})\right)\right)\right]\left(\frac{l}{\lambda}\right)^2\right\}.\end{aligned} \tag{31}$$

The envelope correlations for desired and interference signals (i.e., $\varrho_{\mathcal{S}}(l, \phi_v, \beta_v)$ and $\varrho_{\mathcal{I}}(l, \phi_v, \beta_v)$) can be independently obtained from (31), by using the corresponding set of shape factors. The spatial selectivity of wireless channels is measured in terms of coherence distance (CD); defined as the spatial separation at which the fading channel remains unchanged. The CD (D_c) and coherence time (T_c) can be related as, $T_c = D_c/v_r$. The CD is also defined as the distance at which spatial correlation satisfies, $\varrho_{(.)}(l = D_c) = 0.5$, [14]. Using this definition of CD and definition of spatial correlation in (31), a new definition of CD for characterization of interference and desired signals in a 3-D propagation environment and for Nakagami-m distributed envelopes, can be expressed in simplified form as,

$$\begin{aligned}D_{c_{(.)}} \approx \\ \sqrt{\frac{3\ \ln(2)\lambda^2\left(m_{(.)}\Gamma^2\left(m_{(.)}\right) - \Gamma^2\left(m_{(.)} + \frac{1}{2}\right)\right)}{\Upsilon_{(.)}^2 m_{(.)}\Gamma^2\left(m_{(.)}\right)}}\left\{1 + \frac{3}{2}\right. \\ \times\left(\xi_{(.)}\left(2\sin^2\beta_v - \frac{2}{3}\right) + \chi_{(.)}\cos\left(\phi_v - \phi_{\beta 45_{(.)}}^{\max}\right)\right. \\ \left.\left.\times\sin(2\beta_v) + \zeta_{(.)}\cos^2\beta_v\cos\left(2(\phi_v - \phi_{\beta 0_{(.)}}^{\max})\right)\right)\right\}^{-1/2}.\end{aligned} \tag{32}$$

The envelope correlation for SIR can be obtained in a similar way, as represented for desired/interference signals in (30), which can be obtained as,

$$\varrho_\eta(l, \phi_v, \beta_v) = \frac{\mathbb{E}\left[\Theta_\eta(l)\right] - \mathbb{E}^2\left[\eta\right]}{\mathbb{E}\left[\eta^2\right] - \mathbb{E}^2\left[\eta\right]} \tag{33}$$

where $\Theta_\eta(l) = \eta\{\vec{\mathrm{l}}_0\}\eta\{\vec{\mathrm{l}}_0 + l\hat{\mathrm{l}}\} = \Theta_{\mathcal{S}}^2(l)/\Theta_{\mathcal{I}}^2(l)$. Further, the simplified approximate solution for its expected value, as provided in [12], can be obtained as follows,

$$\mathbb{E}\left[\Theta_\eta(l)\right] = \frac{\mathbb{E}^2\left[\Theta_{\mathcal{S}}(l)\right]}{\mathbb{E}^2\left[\Theta_{\mathcal{I}}(l)\right]} + \frac{3P_{\mathcal{I}}^2\mathbb{E}^2\left[\Theta_{\mathcal{S}}(l)\right]}{m_{\mathcal{I}}\mathbb{E}^4\left[\Theta_{\mathcal{I}}(l)\right]} + \frac{P_{\mathcal{S}}^2}{m_{\mathcal{S}}\mathbb{E}^2\left[\Theta_{\mathcal{I}}(l)\right]}, \tag{34}$$

where $\mathbb{E}\left[\Theta_{\mathcal{I}}(l)\right]$ and $\mathbb{E}\left[\Theta_{\mathcal{S}}(l)\right]$ can be obtained by solving (30). The simplified solution can be expressed as,

$$\begin{aligned}\mathbb{E}\left[\Theta_{(.)}(l)\right] = \varrho_{(.)}(l, \phi_v, \beta_v)\left[P_{(.)} - \frac{P_{(.)}}{m_{(.)}}\right. \\ \left.\times\left(\frac{\Gamma(m_{(.)} + 1/2)}{\Gamma(m_{(.)})}\right)^2\right] + \frac{P_{(.)}}{m_{(.)}}\left(\frac{\Gamma\left(m_{(.)} + 1/2\right)}{\Gamma(m_{(.)})}\right)^2.\end{aligned} \tag{35}$$

where it can be used independently for both desired and interference signals by using corresponding parameters. The expected value of the square of SIR, $\mathrm{E}\left[\eta^2\right]$, can be obtained from the solution provided in [12], which is,

$$\mathrm{E}\left[\eta^2\right] = \left(\frac{m_{\mathcal{S}}P_{\mathcal{I}}}{m_{\mathcal{I}}P_{\mathcal{S}}}\right)^{-2}\frac{\Gamma(m_{\mathcal{S}} + 2)\Gamma(m_{\mathcal{I}} - 2)}{\Gamma(m_{\mathcal{S}})\Gamma(m_{\mathcal{I}})}. \tag{36}$$

IV. RESULTS AND DISCUSSION

This section provides performance evaluation of the proposed methodology for characterization of network interference in 3-D angular domain. The analysis is conducted by following the hypothesis presented in Fig. 2 and 3 for the two-tier HetNet scenario presented in Fig. 1. First, a numerical analysis for validation of the derived analytical expressions is conducted through a comparison of analytical results with performed computer simulations based results. This analysis is performed for a simplified scenario of single interferers' cluster. The initial position of receiver $\mathcal{R}$ is assumed at origin of the coordinate system $(0, 0, 0)$. The cluster of interferers

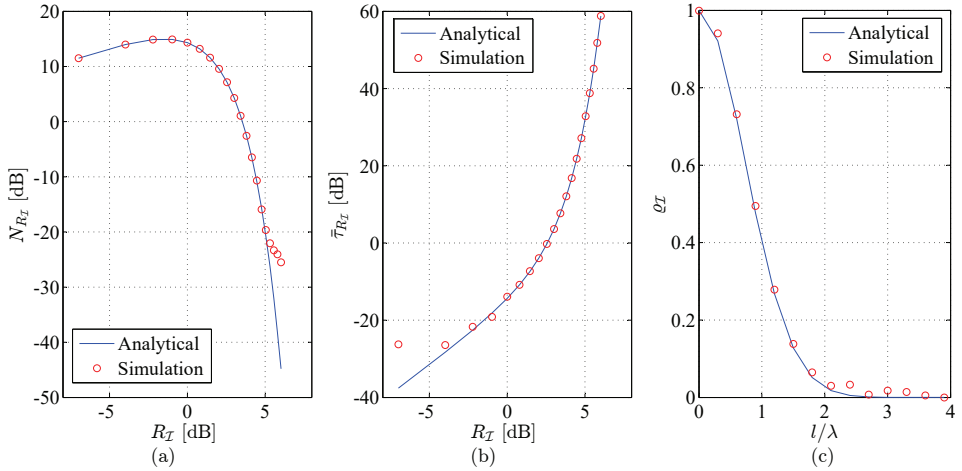

FIGURE 6: Comparison of analytical and simulation results.

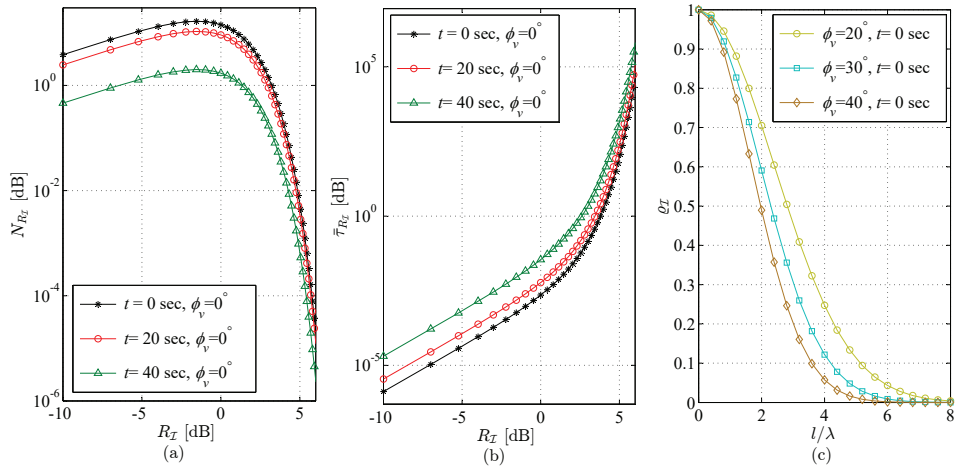

FIGURE 7: The effect of increase in distance (i.e., at time instant $t = 0$sec, $t = 20$sec, and $t = 40$sec) of the receiver from a single cluster of interferers w.r.t. different values threshold level on LCR and AFD in (a) and (b), respectively. The effect of increase in horizontal deviation in position of the receiver from its initial position at $t = 0$sec normalized w.r.t. wavelength is shown on SAC in (c), for different azimuthal direction of receiver's motion.

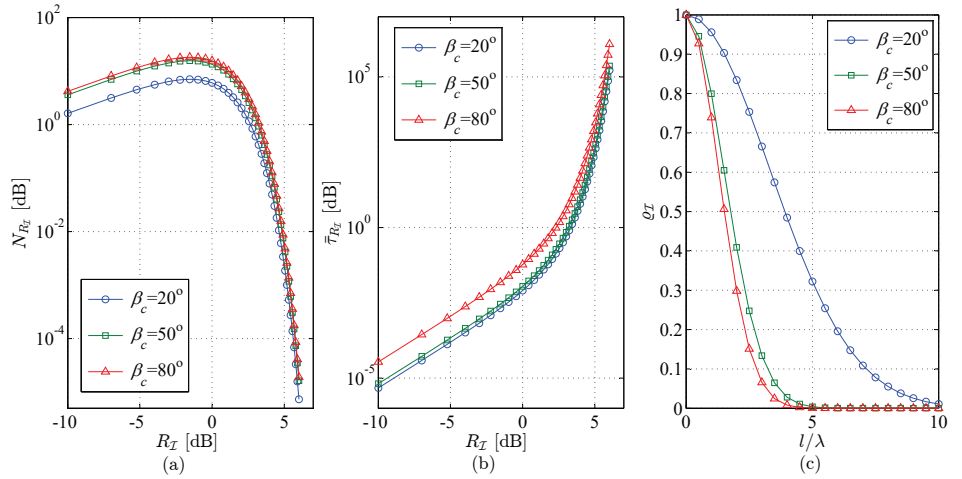

FIGURE 8: Effect of increase in altitude of interferers' cluster on LCR, AFD, and SAC in (a), (b), and (c), respectively.

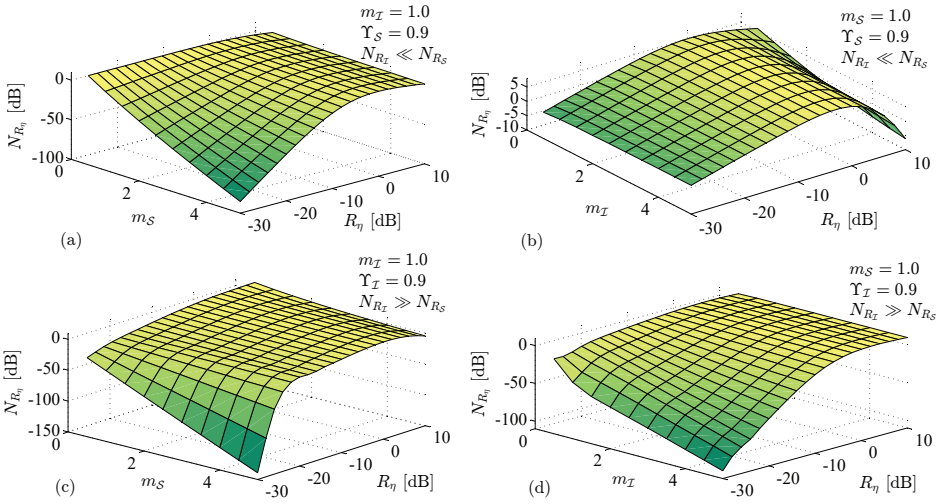

FIGURE 9: The effect of distribution shape parameter of interference ($m_{\mathcal{I}}$) and desired ($m_{\mathcal{S}}$) signals on LCR of SIR threshold level. (a) and (b) demonstrate the case $N_{R_{\mathcal{I}}} \ll N_{R_{\mathcal{S}}}$; (c) and (d) demonstrate the case $N_{R_{\mathcal{I}}} \gg N_{R_{\mathcal{S}}}$.

is taken with radius $\varrho_1 = 200$m positioned (its center) at the coordinates $(-250, 0, 50)$ The receiver is assumed mobile with a velocity $v = 18$m/s in the azimuth plane and at a fixed altitude level, while the x-axis is assumed fixed along the azimuthal direction of the receiver's motion, i.e., $\phi_v = 0°$ and $\beta_v = 0°$. The carrier frequency and path loss exponent are taken as $f_c = 1.8$GHz and $n_{\text{PL}} = 2$, respectively. The position of interferers within the cluster are drawn from homogeneous PPP with an intensity $\lambda_{\mathcal{I}} = 0.02$. The computer simulations are performed by following the approach presented in Chap. 5 of [17] for simulation of wireless propagation channels to characterize second order fading statistics. A time window of 1sec is taken, for simulation results and the results are averaged over 10^4 monte carlo runs. The analytical and simulation results for LCR, AFD, and SAC of interference signals obtained for the single cluster scenario are plotted in Fig. 6 (a), (b), and (c), respectively. A good agreement between the two is observed, which validates the derived analytical expressions. The minor difference in fitting of simulation and analytical results is because the received signal's envelope in analytical results is modeled as pure Rayleigh distributed (as a special case of Nakagami-m distribution); while in the simulation results, the spatial configuration of interferers may result in a slightly different shape of the distribution. A more accurate fitting can be achieved by an appropriate selection of the distribution shape parameter's value (i.e., m) in analytical results or by appropriately setting the spatial configuration of interferers in the simulation setup such that it results in pure Rayleigh distribution of envelope.

The analysis is further extended to study the impact of increasing the ratio between link distance and radius of interfering spheroid's cluster ρ/ρ_c. The results for LCR and AFD at three different positions of the receiver (i.e., $\mathcal{R}$ at time $t = 0$sec, $t = 20$sec, and $t = 40$sec) are plotted in Fig. 7 (a) and (b) respectively. The direction of motion is taken as, $\phi_v = 0°$ and $\beta_v = 0°$, i.e., the receiver moves away from the interfering cluster. the rate of fluctuations in the envelope of receiver interference signal decreases nonlinearly; while the average duration for which the signal stays in a fade increases. The trend of AFD and LCR is observed similar to that commonly observed for different wireless propagation channels. In Fig. 7 (c), SAC is plotted with respect to (w.r.t.) the receiver's displacement from initial position at $t = 0$ sec. The SAC can be studied in terms of separation distance normalized as number of wavelengths and the direction of receivers motion w.r.t. the center of interferers' cluster can be observed. In order to demonstrate the importance of incorporating the elevation axis into the account, the impact of increasing the elevation of interferers' cluster (while keeping the distance same) on LCR, AFD, and SAC of interference signal is plotted in Fig. 8. It can be observed that an increase in elevation angle constituted at the receiver with the center of interferers' cluster (i.e., β_c) has a nonlinear effect along different values of threshold level. The effect of increase in β_c on LCR and AFD become more significant as the threshold level under observation decreases. Furthermore, the effect of increase in elevation of the cluster on SAC is studied for different positions of receiver's (i.e., different values of displacement from initial position in terms of wavelengths). An Increase in separation of the receiver's horizontal position from its initial position decreases the SAC; however this trend of decay becomes sharp for higher values of elevation. These result clearly indicate the importance of not excluding the elevation plane when modeling the HetNets interference in angular domain.

The analytical results for LCR of SIR (N_{R_η}) are plotted in Fig. 9 using the equations (25) and (26) for the special cases discussed in previous section. The maximum crossings occur for the values of SIR around 0dB, and decrease as SIR

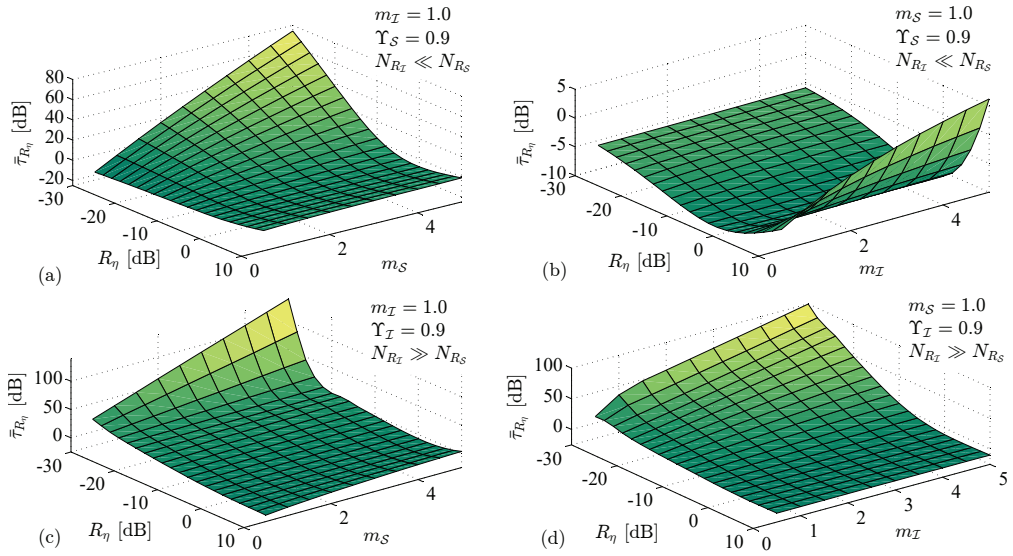

FIGURE 10: The effect of distribution shape parameter of interference ($m_{\mathcal{I}}$) and desired ($m_{\mathcal{S}}$) signals on AFD of SIR threshold level. (a) and (b) demonstrate the case $N_{R_{\mathcal{I}}} \ll N_{R_{\mathcal{S}}}$; (c) and (d) demonstrate the case $N_{R_{\mathcal{I}}} \gg N_{R_{\mathcal{S}}}$.

deviates away from 0dB. The rate of decrease is however different for different cases presented in Fig. 9 (a), (b), (c), and (d). The impact of distribution's shape parameter for both the interference $m_{\mathcal{I}}$ and desired $m_{\mathcal{S}}$ signals is studied for the cases when $N_{R_{\mathcal{I}}} \ll N_{R_{\mathcal{S}}}$ and $N_{R_{\mathcal{I}}} \gg N_{R_{\mathcal{S}}}$. For the case $N_{R_{\mathcal{I}}} \ll N_{R_{\mathcal{S}}}$, when the interference signal is Rayleigh distributed (i.e., $m_{\mathcal{I}} = 1$), an increase in the value of desired signal's distribution's shape parameter, reduces the value of LCR along both tails at low and high values of SIR threshold level, see Fig. 9 (a). However, this impact is more dominant along the lower SIR levels as compared to the higher values. Whereas, varying $m_{\mathcal{I}}$ while keeping the $m_{\mathcal{S}}$ fixed at 1.0, has a converse behaviour in its impact, see Fig. 9 (b). The shape of the curves is observed similar to the shape of LCR commonly observed for Rayleigh distributed signals in wireless propagation channels. On the other hand, when $N_{R_{\mathcal{I}}} \gg N_{R_{\mathcal{S}}}$ and $m_{\mathcal{I}} = 1.0$, an increase in $m_{\mathcal{S}}$ causes a change from flat-shaped LCR over the whole range of SIR to a shape with dips at its tails and flat over middle range of threshold values, evident in Fig. 9 (c). When the desired signal is considered Rayleigh distributed, the effect of varying the shape of interference signal's distribution on LCR of SIR is plotted in Fig. 9 (d). Significant impact on LCR can be observed for lower values of SIR threshold level, where its behaviour is similar to that observed in Fig. 9 (a). The cases studied for characterization of LCR of SIR in Fig. 9, can be further translated to characterize of AFD, as plotted in Fig. 10. For the case, when the rate of fluctuations in interference signal is higher than that in the desired signal, the range of AFD increases significantly with an increase in the value of shape parameter of desired signal's distribution, see Fig. 10(a). The behaviour of increase in AFD along an increase in $m_{\mathcal{S}}$ and a decrease in SIR level is observed to be as linear with different level of slopes and exponential of different orders, respectively. In the results presented in Fig. 10(d) for the case where $N_{R_{\mathcal{I}}} \gg N_{R_{\mathcal{S}}}$, a similar behaviour is observed for a converse set of interference and desired signal parameters as for the case presented in Fig. 10(a). The behaviour of AFD can be related to the behaviour of LCR as inversely proportional to each other, which is evident in the derived formulas and the presented results. This study for characterization of network interference in spatial domain is of high significance for performance evaluation and to meet the challenges in devising of error correction codes and algorithms for interference mitigation in emerging 5G communication scenarios where BSs are employed with very large-scale antenna arrays.

V. CONCLUSION

A novel model for the 3-D angular characterization of the cumulative interference was proposed in a two-tier heterogeneous network with small cells in tier-1 overlaid with massive-MIMO equipped macro-cell BSs in tier-2. Analytical expressions were derived for the second order fading statistics such as the level-crossing rate, the average fade duration, and the correlation distance for Nakagami-m distributed interference and desired signals. Furthermore, analytical expressions for the second order fading statistics of the SIR have also been presented to characterize the behavior of network interference levels with reference to the desired signal. The simplified expressions for these statistics have also been presented for two special cases of practical interest, viz: when the rate of fluctuation of the desired signal is larger than that of the interference signal and vice versa. An analysis of the lifespan of interferer clusters is performed to provide insights into their clustering mechanism in relation to the mobility of the receiver. Finally, a comprehensive evaluation of the impact of various physical and statistical parameters

on second order fading statistics of the interference and the SIR has been presented. Validation of the proposed analytical expressions has been established through a comparison with computer simulations. Our results demonstrate the importance of including the elevation plane in modeling the cumulative interference in HetNets designed for emerging 5G communication scenarios.

ACKNOWLEDGEMENT

The authors would like to acknowledge the financial support by EU ATOM-690750 research project approved under the call identifier H2020-MSCA-RISE-2015.

REFERENCES

[1] K. Hosseini, J. Hoydis, S. T. Brink, and M. Debbah, "Massive MIMO and small cells: How to densify heterogeneous networks," in proc. of IEEE Int Conf. on Commun., 2013, pp. 5442–5447.
[2] E. G. Larsson, O. Edfors, F. Tufvesson, and T. L. Marzetta, "Massive MIMO for next generation wireless systems," IEEE Commun. Mag., vol. 52, no. 2, pp. 186–195, 2014.
[3] J. Hoydis, S. T. Brink, and M. Debbah, "Massive MIMO in the UL/DL of cellular networks: How many antennas do we need?" IEEE J. on Sel. Areas in Commun., vol. 31, no. 2, pp. 160–171, 2013.
[4] A. He, L. Wang, M. Elkashlan, Y. Chen, and K. Wong, "Spectrum and energy efficiency in massive MIMO enabled HetNets: A stochastic geometry approach," IEEE Commun. Lett., vol. 19, no. 12, pp. 2294–2297, 2015.
[5] A. Adhikary, H. S. Dhillon, and G. Caire, "Massive-MIMO meets HetNet: Interference coordination through spatial blanking," IEEE J. on Sel. Areas in Commun., vol. 33, no. 6, pp. 1171–1186, 2015.
[6] M. Kountouris and N. Pappas, "HetNets and massive MIMO: Modeling, potential gains, and performance analysis," in proc. of IEEE-APS Topical Conf. on Antennas and Propag. in Wireless Commun., 2013, pp. 1319–1322.
[7] H. S. Dhillon, R. K. Ganti, F. Baccelli, and J. G. Andrews, "Modeling and analysis of *K*-tier downlink heterogeneous cellular networks," IEEE J. on Sel. Areas in Commun., vol. 30, no. 3, pp. 550–560, Apr. 2012.
[8] A. He, L. Wang, Y. Chen, M. Elkashlan, and K. Wong, "Massive MIMO in *K*-tier heterogeneous cellular networks: Coverage and rate," in proc. of IEEE Global Commun. Conf. IEEE, 2015, pp. 1–6.
[9] X. Jia, M. Zhou, L. Yang, and H. Zhu, "Stochastic geometry based asymptotic analysis for two-tier HetNets with massive MIMO relay employing MRC/MRT and ZF processing," Trans. on Emerging Telecomm. Tech., vol. 28, no. 4, 2017.
[10] J. Dommel, P. P. Knust, L. Thiele, and T. Haustein, "Massive MIMO for interference management in heterogeneous networks," in proc. of IEEE Sensor Array and Multichannel Signal Process. Workshop, 2014, pp. 289–292.
[11] K. Gulati, B. L. Evans, J. G. Andrews, and K. R. Tinsley, "Statistics of co-channel interference in a field of poisson and poisson-poisson clustered interferers," IEEE Trans. on Signal Process., vol. 58, no. 12, pp. 6207–6222, Dec. 2010.
[12] Y. Chen, L. Mucchi, R. Wang, and K. Huang, "Modeling network interference in the angular domain: Interference azimuth spectrum," IEEE Trans. on Commun., vol. 62, no. 6, pp. 2107–2120, Jun. 2014.
[13] J. G. Andrews, R. K. Ganti, M. Haenggi, N. Jindal, and S. Weber, "A primer on spatial modeling and analysis in wireless networks," IEEE Commun. Mag., vol. 48, no. 11, 2010.
[14] G. D. Durgin and T. S. Rappaport, "Theory of multipath shape factors for small-scale fading wireless channels," IEEE Trans. on Antenna and Propag., vol. 48, no. 5, pp. 682–693, May 2000.
[15] D. G. Valchev and D. Brady, "Three-dimensional multipath shape factors for spatial modeling of wireless channels," IEEE Trans. on Wireless Commun., vol. 8, no. 11, pp. 5542–5551, Nov. 2009.
[16] S. J. Nawaz, N. M. Khan, and R. Ramer, "3-D spatial spread quantifiers for multipath fading wireless channels," IEEE Wireless Commun. Lett., vol. 5, no. 9, pp. 484–487, Jul. 2016.
[17] F. P. Fontán and P. M. Espiñeira, Modeling the wireless propagation channel: A simulation approach with MATLAB. John Wiley & Sons, 2008, vol. 5.
[18] N. M. Khan, "Modeling and characterization of multipath fading channels in cellular mobile communication systems," Ph.D. dissertation, University of New South Wales, 2006.
[19] S. J. Nawaz, S. Wyne, K. B. Baltzis, S. M. Gulfam, and K. Cumanan, "A tunable 3-D statistical channel model for spatio-temporal characteristics of wireless communication networks," Transactions on Emerging Telecommunications Technologies, p. e3213, 2017.
[20] K. I. Pedersen, P. E. Mogensen, and B. H. Fleury, "A stochastic model of the temporal and azimuthal dispersion seen at the base station in outdoor propagation environments," IEEE Trans on Veh. Technol., vol. 49, no. 2, pp. 437–447, Mar 2000.
[21] P. Petrus, J. H. Reed, and T. S. Rappaport, "Geometrical-based statistical macrocell channel model for mobile environments," IEEE Trans. on Commun., vol. 50, no. 3, pp. 495–502, Mar. 2002.
[22] S. J. Nawaz, M. N. Patwary, N. M. Khan, and H. Yu, "3-D Gaussian scatter density propagation model employing a directional antenna at BS," in proc. of 5th Adv. Satellite Multimedia Syst. Conf. and the 11th Signal Process. for Space Commun. Workshop, 2010, pp. 395–400.
[23] S. J. Nawaz, B. H. Qureshi, and N. M. Khan, "A generalized 3-D scattering model for a macrocell environment with a directional antenna at the BS," IEEE Trans. on Veh. Technol., vol. 59, no. 7, pp. 3193–3204, Sep. 2010.
[24] S. J. Nawaz, N. M. Khan, M. N. Patwary, and M. Moniri, "Effect of directional antenna on the Doppler spectrum in 3-D mobile radio propagation environment," IEEE Trans. on Veh. Technol., vol. 60, no. 7, pp. 2895–2903, Sep. 2011.
[25] J. F. Paris and D. M. Jimenez, "Outage probability analysis for Nakagami-*q* (Hoyt) fading channels under Rayleigh interference," IEEE Trans. on Wireless Commun., vol. 9, no. 4, pp. 1272–1276, Apr. 2010.
[26] M. D. Yacoub, J. E. V. Bautista, and L. G. de Rezende Guedes, "On higher order statistics of the nakagami-m distribution," IEEE Trans. on Veh. Technol., vol. 48, no. 3, pp. 790–794, 1999.

Syed Junaid Nawaz (S'08–M'12–SM'16) received the B.Sc. and M.Sc. degrees in computer engineering from COMSATS Institute of Information Technology (CIIT) Abbottabad, in Aug. 2005 and Feb. 2008, respectively. Since Sep. 2005, he has worked on several research and teaching positions with CIIT Abbottabad, CIIT Islamabad, Federal Urdu University Pakistan, Staffordshire University UK, and Aristotle University of Thessaloniki Greece. He is currently working as an Assistant Professor with the Department of Electrical Engineering, CIIT Islamabad. He received the Ph.D. degree in electronic engineering from Mohammad Ali Jinnah University Islamabad, in Feb. 2012. He has an active presence in the research community through publications in reputed international journals and conferences in different areas of wireless communications. His current research interests include physical channel modeling and characterization, interference modeling, channel estimation and equalization, massive MIMO systems, compressive sensing, vehicle-to-vehicle communications, airborne internet, and adaptive signal processing.

Abrar Ahmed was born in Pakistan in 1985. He received his BS in Computer Engineering in 2006 from COMSATS Institute of Information Technology, Abbottabad, Pakistan. In 2008, he received his MS degree from Lancaster University, UK. He received his Ph.D. degree in electronic engineering from COMSATS Institute of Information Technology, Islamabad in August 2017. He is associated with COMSATS Institute of Information Technology, Islamabad since 2006 and currently holds the position of Assistant Professor. His research interests include wireless channel modeling and characterizing, smart antenna systems, non-orthogonal multiple access techniques, and adaptive signal processing.

Shurjeel Wyne (S'02–M'08–SM'13) received his Ph.D. from Lund University, Sweden in March 2009. Between April 2009 and April 2010, he was a Post-Doctoral Research Fellow funded by the High-Speed Wireless Centre at Lund University. Since June 2010 he is with the Department of Electrical Engineering at COMSATS Institute of Information Technology, Islamabad, Pakistan, where he serves as an Associate Professor. His research interests include wireless channel measurements and modeling, relay networks, Multiple-input Multiple-output (MIMO) systems, physical layer security, and wireless information and power transfer. He is a Co-recipient of the best paper award of the Antennas and Propagation Track in IEEE VTC2013-Spring.

Kanapathippillai Cumanan (M'10) received the B.Sc. (Hons.) degree in electrical and electronic engineering from the University of Peradeniya, Sri Lanka, in 2006, and the Ph.D. degree in signal processing for wireless communications from Loughborough University, Loughborough, U.K., in 2009. He is currently a Lecturer with the Department of Electronics, University of York, U.K. He was with the School of Electronic, Electrical and System Engineering, Loughborough University, U.K. He was a Teaching Assistant with the Department of Electrical and Electronic Engineering, University of Peradeniya, Sri Lanka, in 2006. In 2011, he was an Academic Visitor with the Department of Electrical and Computer Engineering, National University of Singapore, Singapore. He was a Research Associate with the School of Electrical and Electronic Engineering, Newcastle University, U.K., from 2012 to 2014. His research interests include physical layer security, cognitive radio networks, relay networks, convex optimization techniques, and resource allocation techniques. He was a Research Student with Cardiff University, Wales, U.K., from 2006 to 2007. He was a recipient of an Overseas Research Student Award Scheme from Cardiff University.

Zhiguo Ding (S'03–M'05–SM'15) received the B.Eng. degree from Beijing University of Posts and Telecommunications, Beijing, China, in 2000 and the Ph.D. degree from Imperial College London, London, U.K., in 2005, both in electrical engineering. From July 2005 to August 2014, he was with QueenâĂŹs University Belfast, Imperial College London, and Newcastle University. Since September 2014, he has been a Chair Professor with Lancaster University, Lancashire, U.K. From October 2012 to September 2016, he was an academic visitor with Princeton University, Princeton, NJ, USA. His research interests include 5G networks, game theory, cooperative and energy-harvesting networks, and statistical signal processing. Dr. Ding is an Editor for the IEEE TRANSACTIONS ON COMMUNICATIONS, the IEEE TRANSACTIONS ON VEHICULAR TECHNOLOGY, IEEE WIRELESS COMMUNICATION LETTERS, IEEE COMMUNICATION LETTERS, and the Journal of Wireless Communications and Mobile Computing. He received the Best Paper Award at the 2009 IET Communication Conference on Wireless, Mobile, and Computing; IEEE COMMUNICATIONS LETTER Exemplary Reviewer in 2012; and the EU Marie Curie Fellowship during 2012âĂŞ2014.